SIAM J. APPL. MATH.
Vol. 70, No. 3, pp. 923–948

MOTION OF A YAWED SUPERCAVITATING WEDGE BENEATH A FREE SURFACE*

Y. A. ANTIPOV† AND A. Y. ZEMLYANOVA†

Abstract. The problem that is studied concerns a yawed wedge under a free surface, moving at a uniform speed. The model involves a trailing cavity whose boundary is a dividing streamline through the vertex of the wedge. The cavity closure mechanism is described according to the Tulin–Terent'ev single-spiral-vortex model. A closed-form solution to the governing nonlinear boundary-value problem is found by the method of conformal mappings. The doubly connected flow domain is treated as the image by this map of the exterior of two slits in a parametric plane. The mapping function is constructed through the solution to two boundary-value problems of the theory of analytic functions, the Hilbert problem for two slits in a plane, and the Riemann–Hilbert problem on an elliptic surface. Numerical results for the shape of the cavity and the free surface, the yaw angle, the drag and lift coefficients, and the circulation are reported.

Key words. Riemann–Hilbert program, Reimann surfaces, conformal map, supercavitation, free surface

AMS subject classifications. 76B10, 30C20, 35Q15

DOI. 10.1137/090747300

1. Introduction.

The flow induced by the motion of a body and the formation of a trailing cavity (also known as a supercavity) are of considerable interest in marine applications such as the design and analysis of hydrofoils and marine propellers. In order to design a cavitating hydrofoil system operating near a free surface, it is required to analyze the cavity shape and the profile of the free surface and understand how the presence of the free surface and the cavity affects the performance of the body.

The central problem in the modeling of supercavitating flow is to describe the cavity closure mechanism for finite cavities and to recover the cavity shape. The existing steady-state models assume that the boundary of the cavity is a free streamline and propose a mechanism to avoid the Brillouin paradox. This paradox states that a bounded closed cavity with constant pressure cannot be reconstructed in the framework of the ideal flow theory. A survey of the literature on cavitating flow, including the analysis of most commonly used cavity closure models, can be found in [6], [26], [27], [7], [10]. None of the known steady-state cavitating models, linear and nonlinear, are exact. An approximate nonlinear closed-cavity model was proposed in [20]. This model assumes the existence of a transition zone in the rear part of the cavity, where the velocity, and therefore pressure, is not constant and obeys a certain law. An algebraic law was used in [17] to design a numerical code based on the boundary integral method for the analysis of 2d and 3d partial (sheet) cavitating flow. This model was further developed in [4] in order to solve numerically 2d and 3d problems for cavitating hydrofoils under a free surface.

Some nonlinear models of cavitating flow, flawless from the mathematical point of view, make assumptions which are not always justified from the physical point of

*Received by the editors January 20, 2009; accepted for publication (in revised form) June 5, 2009; published electronically August 12, 2009. This work supported by NSF through grant DMS0707724.
http://www.siam.org/journals/siap/70-3/74730.html

†Department of Mathematics, Louisiana State University, Baton Rouge, LA 70803 (antipov@math.lsu.edu, azem@math.lsu.edu).

view. It is believed [26], however, that the precise details of the flow at the rear part of the cavity have little influence on the flow about the hydrofoil itself. Therefore, the preference for one assumption relative to another one is based on whether an exact or numerical method for the solution is chosen. For all steady-state model problems which can be solved analytically, it is assumed that the pressure is constant everywhere on the cavity boundary, the velocity obeys the Bernoulli law, and the cavity is not closed. In the reentrant-jet model [9], [12], [13], [18], the two branches of the dividing streamline, which define the cavity boundary, reverse direction into the cavity, and a part of main stream flows into a second sheet of a certain two-sheeted Riemann surface. As possible wake and cavity models, Tulin [26] proposed to introduce twin vortices, either single-spiral, or double-spiral. Mathematically, the main difference between the single-spiral-vortex and double-spiral-vortex models is the asymptotics of the solution at the point where the dividing streamlines attempt to close the cavity. Also, at infinity, the flow is not continuous in the former model, while the second model assumes the existence of a semi-infinite wake behind the cavity with a constant speed, the same as at the infinite point. Thus, the flow is continuous at infinity but the velocity is discontinuous at the double-spiral vortices. This means that regardless of the number of foils placed in a strip, a half-plane, or a plane, the double-spiral-vortex model treats the flow domain as a simply connected domain. This circumstance makes this model similar to the Kirchhoff zero-cavitation-number model. The double-spiral-vortex model was used in [19], [15], [11], [5]. Larock and Street analyzed a supercavitating hydrofoil beneath a free surface. The case of two supercavitating foils near a free surface was considered by Green and Street. Furuya reduced the problem for an arbitrary-shaped supercavitating foil under a free surface to a nonlinear integral equation and solved it numerically. Bassanini and Elcrat employed the method of conformal mappings for a polygonal supercavitating foil in a plane.

According to the Tulin single-spiral-vortex model [26], the complex velocity potential has a singularity given by $\ln w'(z) \sim [w(z) - w(C)]^{-1/2}$, $z \to C$. Here C is a point between C^- and C^+, where the two branches of the streamline attempt to close the cavity. Based on the Brillouin condition $V < V_1$, where V and V_1 are the flow speeds on the cavity boundary and in the flow domain, respectively, Terent'ev [23] proved that, in fact, $\ln w'(z) \sim -K[w(z) - w(C)]^{-1/2}$, $z \to C$, $-\pi \le \arg[w(z) - w(C)] \le \pi$, K is a positive factor. The branch of the square root is chosen such that $[w(z)-w(C)]^{1/2} > 0$ when $\arg[w(z)-w(C)] = 0$. Another difference between the Tulin model and its modification by Terent'ev is that the circulation Γ is zero in the Tulin model while it is not fixed a priori in its modification by Terent'ev. The presence of the two extra parameters, K and Γ, makes it possible to satisfy the complex condition $\int_{L_1} dz = 0$ (this condition is not met by the Tulin model). Here L_1 is the combined boundary of the cavity and the hydrofoil.

This model and the hodograph method were employed in [24] to derive an asymptotic solution for small angles of attack in the case of a supercavitating plate beneath a free surface. Recently [2], a closed-form solution for a supercavitating wedge in a plane was found by the method of the Riemann–Hilbert problem on a complex plane (a genus-0 Riemann surface). A genus-2 case (two supercavitating foils in a channel) was analyzed in [1]. We emphasize that the method [1] ultimately leads to a Jacobi inversion problem for a genus-2 Riemann surface. It turns out that the solution to the Jacobi problem lies on the contour of the Riemann–Hilbert problem that is not convenient for numerical purposes. Note that a numerical procedure based on this approach was developed and implemented only for simply connected domains [2].

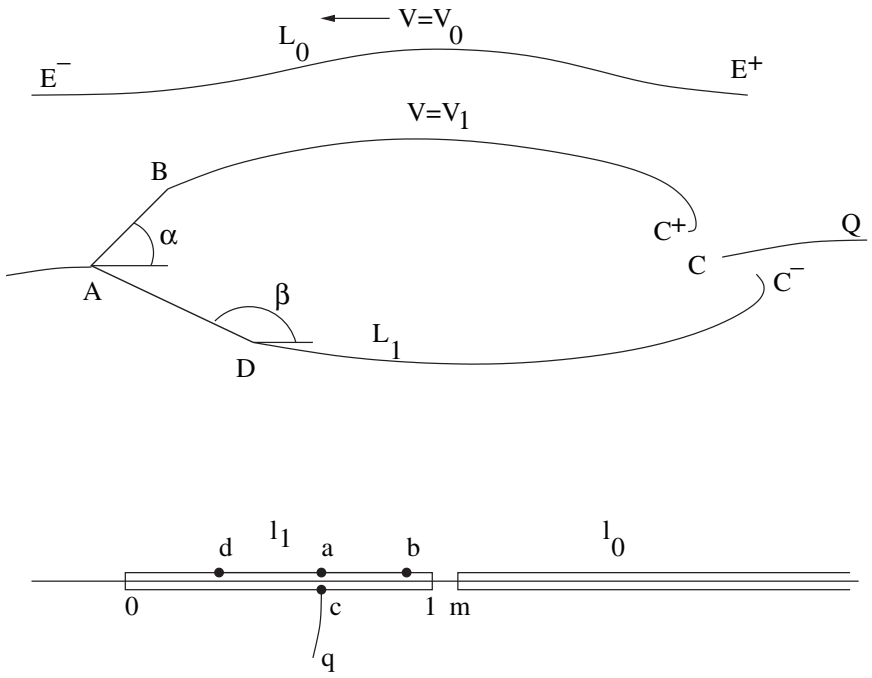

FIG. 1. *The flow domain $\tilde{\mathcal{D}}$ and the parametric domain $\mathcal{D}$.*

The goal of this paper is to derive a closed-form solution to the nonlinear Tulin–Terent'ev model for a supercavitating wedge, BAD, moving with a uniform speed beneath a free surface. We use a function $z = f(\zeta)$ to map a parametric plane with two cuts, $[0, 1]$ and $[m, \infty)$, into the flow domain such that the image of the finite cut is the boundary of the wedge combined with the cavity boundary, and the semi-infinite cut is mapped into the free surface. We express the derivative $df/d\zeta$ through two functions $\omega_0(\zeta)$ and $\omega_1(\zeta)$. The former function is found through the solution of a Hilbert problem for two cuts on the parametric plane. The function $\omega_1(\zeta)$ is recovered through the solution of a certain Riemann–Hilbert problem on an elliptic surface. Its solution is found by quadratures, and the associated Jacobi inversion problem is solved in terms of elliptic functions. The final formulas for the mapping function possess four unknowns, a, b, and d, the preimages of the edging points A, B, and D, respectively, and the parameter m (it is proved that $c = \bar{a}$). We develop a Newton-type numerical procedure for the nonlinear system and discuss numerical results for the cavity and the free surface profiles, the angle of yaw, the drag and lift coefficients, the singularity factor K, and the circulation.

2. Mathematical formulation. The work is concerned with the motion of a wedge DAB under a free fluid surface (Figure 1). Far away from the wedge, the calm free surface is described by $x_2 = h$. At time t, the vertex A is located at the point $x_1 = -V_0 t$, $x_2 = 0$, and the wedge is moving with uniform speed, V_0, in the negative direction. The speed V_0 is much smaller than the sound speed, and the fluid may be considered as an incompressible liquid. The geometry of the wedge is described by four parameters, λ_1, λ_2, α_0, and β_0, where λ_1 and λ_2 are the lengths of the sides AB and AD, and α_0 and β_0 are the angles the upper and lower faces of the wedge initially form with the x_1-axis, respectively. The fluid is assumed to be inviscid and

irrotational. Gravity is neglected. It is also assumed that the wedge may move about the z-axis passing through the point A and orthogonal to the 2d flow domain. The angle of yaw, δ, is to be determined from the condition that the front stagnation point coincides with the vertex A. This means that the actual location of the wedge ends is described by the angles $\alpha = \alpha_0 + \delta$ and $\beta = \beta_0 + \delta$. The dividing streamline through the point A traverses the upper and lower faces of the wedge, breaks away at the rear points B and D, and forms the upper and lower boundaries, BC^+ and DC^-, of a cavity behind the wedge.

For the problem of concern, it is desirable to employ a coordinate system that moves with the wedge. Thus we introduce

$$x = x_1 + V_0 t, \quad y = x_2, \quad z = x + iy, \tag{2.1}$$

and define the complex velocity potential $w(z) = \phi(z) + i\psi(z)$, $z \in \tilde{\mathcal{D}}$, and the complex conjugate velocity, $dw/dz = u_x - iu_y$. Here ϕ is the velocity potential, ψ is the stream function, $\tilde{\mathcal{D}}$ is the flow domain, and $\mathbf{v} = (u_x, u_y)$ is the velocity vector. The function $w(z)$ is analytic in the flow domain $\tilde{\mathcal{D}}$, and it satisfies the following boundary conditions:

$$\begin{gathered} \operatorname{Im} w(z) = C_j, \quad z \in L_j, \quad j = 0, 1, \\ \left|\frac{dw}{dz}\right| = \begin{cases} V_0, & z \in L_0, \\ V_1, & z \in BC^+ \cup DC^-, \end{cases} \\ \arg \frac{dw}{dz} = \begin{cases} -\alpha, & z \in AB, \\ \pi - \beta, & z \in AD, \end{cases} \end{gathered} \tag{2.2}$$

where C_0 and C_1 are real constants not necessarily the same, $L_0 = E^- E^+$ is the free surface, and the contour L_1 consists of the boundary of the cavity $BC^+ \cup DC^-$ and the faces of the wedge DAB. The first condition in (2.2) means that the free surface L_0 and the contour L_1 are some streamlines $\psi(x, y) = C_0$ and $\psi(x, y) = C_1$, respectively. The second condition is due to the fact that the speeds of the motion along the free surface, V_0, and the cavity boundary, $V_1 = \sqrt{\sigma + 1} V_0$, are constant and prescribed. Here σ is the cavitation number

$$\sigma = \frac{p_0 - p_1}{\frac{1}{2}\rho V_0^2}, \tag{2.3}$$

ρ is the density of the liquid, p_1 is the pressure inside the cavity, and p_0 is the water pressure far away from the wedge. The last condition in (2.2) means that the flow is tangential to the wedge faces (the walls of the wedge are assumed to be rigid).

There are two singular points, A and C, in the model. The former point is the front stagnation point, and $dw/dz = 0$ at $z = A$. The second point C is a point where the upper and lower streamlines attempt to close the cavity. This point is unknown a priori and will be recovered from the solution. According to the single-spiral-vortex model in the Terent'ev interpretation [24], the two branches of the dividing streamline reach the two vortices behind the foil, C^+ and C^-, and then pass to a half of an infinitely sheeted Riemann surface of the logarithmic function with the branch points C^+ and C^-. After that the same streamline emerges from the infinite sheet of the Riemann surface and returns to the first, physical, sheet. The streamlines that are close to the boundary of the cavity traverse first around the cavity and then pass to the Riemann surface. After they have traversed a finite number of sheets of the Riemann surface, the streamlines return to the physical sheet.

At a neighborhood of the point C we assume that

$$\log \frac{dw}{dz} = O\left((w - w(C))^{-1/2}\right), \quad z \to C. \tag{2.4}$$

It will later be shown that condition (2.4) leads to the Tulin–Terent'ev condition

$$\log \frac{dw}{dz} \sim -K\left((w - w(C))^{-1/2}\right), \quad z \to C, \quad -\pi \le \arg[w(z) - w(C)] \le \pi. \tag{2.5}$$

Here K is a positive constant, and the branch of the square root is chosen such that $[w(z) - w(C)]^{1/2} > 0$ when $\arg[w(z) - w(C)] = 0$.

The flow domain $\tilde{\mathcal{D}}$ is doubly connected, and the solution to the nonlinear problem (2.2) is very much aided by mapping the entire boundary of the flow into the exterior of two cuts, $l_1 = [0, 1]$ and $l_0 = [m, \infty)$; m is a parameter to be fixed, $1 < m < \infty$ (Figure 1). Let $z = f(\zeta)$ be a conformal map of a parametric ζ-plane cut along the segments l_1 and l_0 onto the flow domain $\tilde{\mathcal{D}}$ such that the cuts l_1 and l_0 are mapped onto the cavity boundary L_1 and the free surface L_0, respectively. Let some boundary points a, b, c, and d of the cut l_1 fall into the points A, B, C, and D, respectively, and a point $e_\infty \in l_0$ fall into the infinite point of the flow domain. Such a map always exists, and it is defined up to one real parameter. Choose $e_\infty = \infty$. Define next the derivative $df/d\zeta$ of the conformal mapping through the derivative $dw/d\zeta$ and the logarithmic hodograph variable by

$$\frac{df}{d\zeta} = \omega_0(\zeta) e^{-\omega_1(\zeta)}, \tag{2.6}$$

where

$$\omega_0(\zeta) = \frac{dw}{V_0 d\zeta}, \quad \omega_1(\zeta) = \ln \frac{dw}{V_0 dz}. \tag{2.7}$$

Our next step is to show that these two functions, $\omega_0(\zeta)$ and $\omega_1(\zeta)$, provide the solutions to two boundary-value problems of the theory of analytic functions, a Hilbert problem on a plane and a Riemann–Hilbert problem on an elliptic Riemann surface.

3. Hilbert problem for the function $\omega_0(\zeta)$. Because of the first boundary condition (2.2), the imaginary part of the function $\omega_0(\zeta)$ vanishes at the banks of the cuts l_0 and l_1:

$$\operatorname{Im} \omega_0(\xi) = 0, \quad \xi \in l_0 \cup l_1. \tag{3.1}$$

In the domain $\mathcal{D} = \mathbb{C} \setminus (l_0 \cup l_1)$, the function $\omega_0(\zeta)$ is analytic. At the point $\zeta = a$ this function has a simple zero [1], [2]. Since the infinite point of the parametric plane is mapped into the infinite point of the physical plane, and $dw/dz \to V_0$ as $z \to \infty$, it follows from (2.6) and (2.7) that

$$\omega_0(\zeta) \sim \frac{df}{d\zeta} = O\left(\zeta^{-1/2}\right), \quad \zeta \to \infty. \tag{3.2}$$

The most general form of the function analytical in the domain $\mathcal{D}$, decaying at infinity as (3.2) and vanishing at the point $\zeta = a$ is [22], [8]

$$\omega_0(\zeta) = N\tilde{\omega}_0(\zeta), \quad \tilde{\omega}_0(\zeta) = \frac{i(\zeta - a)}{p^{1/2}(\zeta)}, \tag{3.3}$$

where N is an arbitrary real constant, and $p(\zeta) = \zeta(1-\zeta)(\zeta - m)$. The function $p^{1/2}(\zeta)$ is analytic in the ζ-plane cut along the lines l_1 and l_0. Its single branch is fixed by the condition $p^{1/2}(\zeta) = i\sqrt{|p(\xi)|}$ as $\zeta = \xi + i0$, $\xi > m$. This branch has the following properties:

$$
\begin{aligned}
&p^{1/2}(\zeta) = \pm i\sqrt{|p(\xi)|}, \quad \zeta = \xi \pm i0, \quad m < \xi < +\infty,\\
&p^{1/2}(\zeta) = -\sqrt{|p(\xi)|}, \quad \zeta = \xi, \quad 1 < \xi < m,\\
&p^{1/2}(\zeta) = \mp i\sqrt{|p(\xi)|}, \quad \zeta = \xi \pm i0, \quad 0 < \xi < 1,\\
&p^{1/2}(\zeta) = \sqrt{|p(\xi)|}, \quad \zeta = \xi, \quad -\infty < \xi < 0.
\end{aligned} \tag{3.4}
$$

At the point c, the preimages bc, dc, and cq of the three branches of the same streamline, BC^+, DC^-, and CQ, respectively, meet, and the function $\omega_0(\zeta)$ has the following asymptotics [2]:

$$\omega_0(\zeta) \sim K_c(\zeta - c), \quad \zeta \to c \quad K_c = \text{const}. \tag{3.5}$$

Thus, the function $\omega_0(\zeta)$ must have a simple zero at the point $\zeta = c \neq a$. It is evident that the only way to meet this requirement is to put $c = \bar{a}$. Now, to fix the constant N, we use the conservation of mass law to a closed contour E^-EAE_0 between two streamlines E^-E_0 and EA. Here $E^- = -\infty + ih$, $E = -\infty + i0$, $A = 0$, and E_0 is a finite point on the free surface. This results in the following relation:

$$V_0 h = \operatorname{Im} \int_{ae_0} \frac{dw}{d\zeta} d\zeta, \tag{3.6}$$

(e_0 is the preimage of the point E_0) or, equivalently,

$$N = h \left(\operatorname{Im} \int_1^m \tilde{\omega}_0(\xi) d\xi \right)^{-1}. \tag{3.7}$$

Here we used the fact that the function $\tilde{\omega}_0(\zeta)$ is real on the banks of the cuts l_0 and l_1 (it is pure imaginary on the segment $[1, m]$). Thus, we have found that $a = \bar{c}$ and that the function $\omega_0(\zeta)$ is defined up to two real parameters, a and m.

4. Riemann–Hilbert problem on an elliptic surface for the function $\omega_1(\zeta)$. The function $\omega_1(\zeta)$ is analytic in the domain $\mathcal{D}$, and because of its definition (2.7) and the boundary conditions (2.2) we have

$$
\begin{aligned}
&\operatorname{Re} \omega_1(\zeta) = \begin{cases} \sigma', & \zeta \in bcd, \\ 0, & \zeta \in l_1, \end{cases} \qquad \sigma' = \log \sqrt{\sigma + 1},\\
&\operatorname{Im} \omega_1(\zeta) = \begin{cases} -\alpha, & \zeta \in ab, \\ \pi - \beta, & \zeta \in da. \end{cases}
\end{aligned} \tag{4.1}
$$

As z approaches the infinite point, $dw/dz \to V_0$, and therefore, $\omega_1(\zeta) \to 0$ as $\zeta \to \infty$. At the stagnation point $z = A$, the velocity vanishes, and hence the function $\omega_1(\zeta)$ has a logarithmic singularity at the point $\zeta = a$. From (2.4), in a neighborhood of the point c, the function $\omega_1(\zeta)$ has the following singularity:

$$\omega_1(\zeta) = O\left([w(z) - w(C)]^{-1/2} \right), \quad z \to C. \tag{4.2}$$

This implies [1] that the function $\omega_1(\zeta)$ is infinite at the point $\zeta = c$,

$$\omega_1(\zeta) = O\left((\zeta - c)^{-1} \right), \quad \zeta \to c. \tag{4.3}$$

We shall identify the point $\zeta = c$ as a pole of the function $\omega_1(\zeta)$. However, this definition does not coincide with the classical one since $\zeta = c$ is a boundary point of the contour l_1 where the function is not analytic. To determine the function $\omega_1(\zeta)$, we reduce the problem (4.1) to a Riemann–Hilbert problem on an elliptic surface.

Let $\mathcal{R}$ be a genus-1 Riemann surface defined by the algebraic equation

$$u^2 = p(\zeta), \quad p(\zeta) = \zeta(1-\zeta)(\zeta - m). \tag{4.4}$$

The surface is formed by gluing two copies $\mathbb{C}_1$ and $\mathbb{C}_2$ of the extended complex ζ-plane $\mathbb{C} \cup \{\infty\}$ cut along the segments l_1 and l_0. The upper sides l_j^+ of the cuts $l_j \subset \mathbb{C}_1$ are glued to the lower sides l_j^- of the cuts $l_j \subset \mathbb{C}_2$, and the sides $l_j^- \subset \mathbb{C}_1$ are glued to $l_j^+ \subset \mathbb{C}_2$ $(j = 0, 1)$. The function $u(\zeta)$ is single-valued on $\mathcal{R}$:

$$u = \begin{cases} p^{1/2}(\zeta), & (\zeta, u) \in \mathbb{C}_1, \\ -p^{1/2}(\zeta), & (\zeta, u) \in \mathbb{C}_2. \end{cases} \tag{4.5}$$

Here $p^{1/2}(\zeta)$ is the same branch as the one fixed in section 3. The pairs $(\zeta, p^{1/2}(\zeta))$ and $(\zeta, -p^{1/2}(\zeta))$ correspond to the points with affix ζ lying on the upper and lower sheets, $\mathbb{C}_1$ and $\mathbb{C}_2$, respectively. The sides of the contour $\mathcal{L} = l_0 \cup l_1$ form the symmetry line for the elliptic surface $\mathcal{R}$ which splits the surface into two symmetric halves. This fact is expressed by the relation between two symmetric points $(\zeta, u) \in \mathbb{C}_1$ and $(\zeta_*, u_*) \in \mathbb{C}_2$: $(\zeta_*, u_*) = (\bar{\zeta}, -u(\bar{\zeta}))$.

Introduce next the following auxiliary function:

$$\Phi(\zeta, u) = \begin{cases} -i\omega_1(\zeta), & (\zeta, u) \in \mathbb{C}_1, \\ i\,\overline{\omega_1(\bar{\zeta})}, & (\zeta, u) \in \mathbb{C}_2. \end{cases} \tag{4.6}$$

It is directly verified that this function satisfies the symmetry condition

$$\overline{\Phi(\zeta_*, u_*)} = \Phi(\zeta, u), \quad (\zeta, u) \in \mathcal{R}. \tag{4.7}$$

On the symmetry line $\mathcal{L}$, we can define the boundary values of the function $\Phi(\zeta, u)$,

$$\begin{aligned} &\Phi^+(\xi, v) = -i\omega_1(\xi) = -i\,\mathrm{Re}\,\omega_1(\xi) + \mathrm{Im}\,\omega_1(\xi), \\ &\Phi^-(\xi, v) = i\overline{\omega(\xi)} = i\,\mathrm{Re}\,\omega_1(\xi) + \mathrm{Im}\,\omega_1(\xi), \quad (\xi, v) \in \mathcal{L}, \quad v = u(\xi), \end{aligned} \tag{4.8}$$

where $\Phi^+(\xi, v)$ $(\Phi^-(\xi, v))$ is the limiting value of the function $\Phi(\zeta, u)$ on the contour $\mathcal{L}$ from the upper (lower) sheet of the surface. The boundary conditions (4.1) therefore imply that the function $\Phi(\zeta, u)$ is the solution to the following Riemann–Hilbert problem.

Find all functions $\Phi(\zeta, u)$ analytic in $\mathcal{R} \setminus \mathcal{L}$, Hölder-continuous up to the boundary $\mathcal{L}$ apart from the singular points $a, b, c,$ and d, with the boundary values satisfying the relation

$$\Phi^+(\xi, v) = G(\xi, v)\Phi^-(\xi, v) + g(\xi, v), \quad (\xi, v) \in \mathcal{L}, \tag{4.9}$$

and the symmetry condition $\overline{\Phi(\zeta_*, u_*)} = \Phi(\zeta, u)$. Here

$$G(\xi, v) = \begin{cases} -1, & (\xi, v) \in dab, \\ 1, & (\xi, v) \in bcd \cup l_0, \end{cases} \qquad g(\xi, v) = \begin{cases} -2\alpha, & (\xi, v) \in ab, \\ 2(\pi - \beta), & (\xi, v) \in da, \\ -2i\sigma', & (\xi, v) \in bcd, \\ 0, & (\xi, v) \in l_0. \end{cases} \tag{4.10}$$

The function $\Phi(\zeta, u)$ has a logarithmic singularity at the point $(a, u(a))$, and a simple pole at the point $(c, u(c))$. It is bounded at the points $(b, u(b))$ and $(d, u(d))$, and $\Phi(\zeta, u) \to 0$ as $\zeta \to \infty$.

4.1. Factorization of the function G. We first find a piecewise meromorphic function $X(\zeta,u)$ which is symmetric on the surface, $X(\zeta,u)=\overline{X(\bar\zeta,-u(\bar\zeta))}$, $(\zeta,u)\in\mathcal{R}\setminus\mathcal{L}$, discontinuous through the contour $dab\in\mathcal{R}$, and whose boundary values on the contour are linked by

$$X^+(\xi,v)=-X^-(\xi,v),\quad (\xi,v)\in dab. \tag{4.11}$$

By using the Weierstrass kernel, an analogue of the Cauchy kernel for the elliptic surface $\mathcal{R}$,

$$dW=\frac{1}{2}\left(1+\frac{u}{v}\right)\frac{d\xi}{\xi-\zeta}, \tag{4.12}$$

we can find a function which meets the boundary condition (4.11),

$$\chi(\zeta,u)=\exp\left\{\frac{1}{4}\int_{dab}\left(1+\frac{u}{v}\right)\frac{d\xi}{\xi-\zeta}\right\}. \tag{4.13}$$

The integration in (4.13) is readily carried out in terms of the Legendre elliptic integral of the third type Π [14],

$$\begin{aligned}\chi(\zeta,u)=&\left(\frac{\zeta-b}{\zeta-d}\right)^{1/4}\\ &\times\exp\left\{\frac{u(\zeta)}{2i\zeta\sqrt{m}}\left[\Pi\left(\sin^{-1}\sqrt{b},\frac{1}{\zeta},\frac{1}{\sqrt{m}}\right)-\Pi\left(\sin^{-1}\sqrt{d},\frac{1}{\zeta},\frac{1}{\sqrt{m}}\right)\right]\right\}.\end{aligned} \tag{4.14}$$

Here $[(\zeta-b)/(\zeta-d)]^{1/4}$ is a fixed branch of the multivalued function.

Analysis of formula (4.12) as $\zeta\to\infty$ shows that the function $\chi(\zeta,u)$ has an essential singularity at infinity. To quench the singularity, we consider the function

$$\chi_0(\zeta,u)=\chi_1(\zeta,u)\overline{\chi_1(\zeta_*,u_*)}, \tag{4.15}$$

where

$$\chi_1(\zeta,u)=\exp\left\{-\frac{1}{2}\left(\int_\gamma+n_a\oint_{\mathbf{a}}+n_b\oint_{\mathbf{b}}\right)\left(1+\frac{u}{v}\right)\frac{d\xi}{\xi-\zeta}\right\}. \tag{4.16}$$

The contour γ is a continuous curve whose starting and terminal points are $\boldsymbol{\eta}_0=(\eta_0,u(\eta_0))$ and $\boldsymbol{\zeta}_0=(\zeta_0,u(\zeta_0))$, respectively. The point $\boldsymbol{\eta}_0$ is an arbitrary fixed point lying on the upper sheet, while the point $\boldsymbol{\zeta}_0$ can lie on either sheet. The point $\boldsymbol{\zeta}_0$ and the integers n_a and n_b are not fixed and are to be recovered from a condition which guarantees the boundedness of the solution to the problem (4.11) at infinity. The contour γ does not cross the **a**- and **b**-cross sections. In the case $\boldsymbol{\zeta}_0\in\mathbb{C}_2$, it passes through the point $\zeta=0$, a branch point of the surface $\mathcal{R}$, and consists of two parts, $(\boldsymbol{\eta}_0,0)\subset\mathbb{C}_1$ and $(0,\boldsymbol{\zeta}_0)\subset\mathbb{C}_2$. If it turns out that the point $\boldsymbol{\zeta}_0$ lies on the upper sheet, then the contour γ can be taken as the straight line joining these points provided it does not cross the segment $[1,+\infty)$.

The system of canonical cross sections $\{\mathbf{a},\mathbf{b}\}$ of the surface $\mathcal{R}$ is chosen as follows. The contour **a** lies on both sheets of the surface and coincides with the banks of the semi-infinite cut l_0 (Figure 2). The loop **b** consists of the segments $[m,1]\subset\mathbb{C}_1$ and $[1,m]\subset\mathbb{C}_2$. The positive direction on the loop **a** is chosen such that the upper sheet is on the left. The loop **a** intersects the loop **b** at the branch point $\zeta=m$ from left

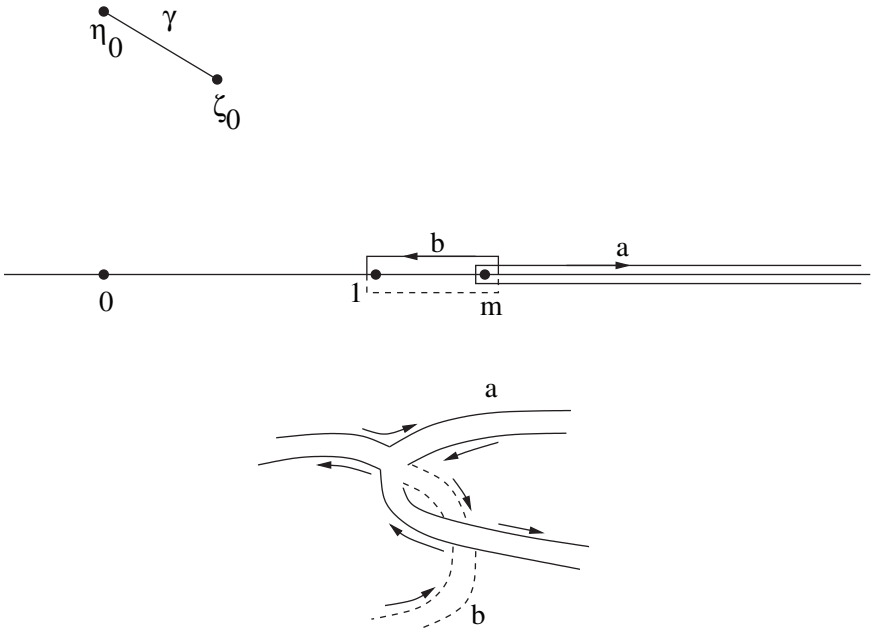

FIG. 2. *The* **a**- *and* **b**-*canonical cross sections and the contour* γ ($\boldsymbol{\zeta}_0 \in \mathbb{C}_1$).

to the right (the positive direction on the cross section **b** is chosen according to the left-hand traffic rule).

Consider now the function $X(\zeta,u)=\chi(\zeta,u)\chi_0(\zeta,u)$. By using the Cauchy theorem, we may simplify the function $X(\zeta,u)$,

$$X(\zeta,u)=\exp\left\{\frac{1}{4}\int_{dab}\left(1+\frac{u(\zeta)}{u(\xi)}\right)\frac{d\xi}{\xi-\zeta}-\frac{1}{2}\int_{\gamma}\left(1+\frac{u(\zeta)}{u(\xi)}\right)\frac{d\xi}{\xi-\zeta}\right.$$
$$\left.-\frac{1}{2}\int_{\gamma}\left(1-\frac{u(\zeta)}{\overline{u(\xi)}}\right)\frac{d\bar{\xi}}{\bar{\xi}-\zeta}-2n_a\int_{\mathbf{a}^+}\frac{u(\zeta)}{u(\xi)}\frac{d\xi}{\xi-\zeta}\right\}, \tag{4.17}$$

where $\mathbf{a}^+=l_0^+$ is the upper bank of the cut l_0. By the Sokhotski–Plemelj formulas, this function satisfies the boundary condition (4.11). The second and the third integrals in (4.17) are discontinuous through the contours γ and γ_*, respectively, where the contour γ_* is symmetric to γ with respect to the line $\mathcal{L}$. The fourth integral is discontinuous through the contour $\mathbf{a}^+$. The jumps are multiples of $2\pi i$, and therefore the function $X(\zeta,u)$ is continuous through the contours γ, γ_*, and $\mathbf{a}^+$. By analyzing the integrals in (4.17) at the points b, d, $\boldsymbol{\eta}_0$, and $\boldsymbol{\zeta}_0$, we find that the function $X(\zeta,u)$ vanishes at the point b, has an integrable singularity at the point d, a simple zero at the point $\boldsymbol{\eta}_0$, and a simple pole at the point $\boldsymbol{\zeta}_0$:

$$X(\zeta,u)=O\left((\zeta-b)^{1/2}\right),\quad \zeta\to b,\quad X(\zeta,u)=O\left((\zeta-d)^{-1/2}\right),\quad \zeta\to d,$$
$$X(\zeta,u)\sim A_0(\zeta-\eta_0),\quad (\zeta,u)\to\boldsymbol{\eta}_0,\quad X(\zeta,u)\sim A_1(\zeta-\zeta_0)^{-1},\quad (\zeta,u)\to\boldsymbol{\zeta}_0. \tag{4.18}$$

Here A_0 and A_1 are nonzero constants. We emphasize that at the conjugate points, $(\bar{b},u(\bar{b}))$, $(\bar{d},u(\bar{d}))$, $(\bar{\eta}_0,u(\bar{\eta}_0))$, and $(\bar{\zeta}_0,u(\bar{\zeta}_0))$, the function $X(\zeta,u)$ is bounded and, in general, does not vanish.

4.2. Jacobi inversion problem. Now, the function $X(\zeta,u)$ must be bounded at infinity. By expanding the integrals in (4.17) in a neighborhood of the two infinite points of the surface $\mathcal{R}$, we find that the necessary and sufficient condition for the boundedness of the function $X(\zeta,u)$ at the infinite points of the surface, $(\infty,\infty)_1$ and $(\infty,\infty)_2$, is

$$\frac{1}{4}\int_{dab}\frac{d\xi}{p^{1/2}(\xi)}-\frac{1}{2}\int_{\gamma}\frac{d\xi}{u(\xi)}+\frac{1}{2}\int_{\gamma}\frac{d\bar{\xi}}{\overline{u(\xi)}}-2n_a\int_{\mathbf{a}^+}\frac{d\xi}{p^{1/2}(\xi)}=0. \tag{4.19}$$

This nonlinear equation with respect to $\boldsymbol{\zeta}_0$ and n_a can be reduced to a Jacobi inversion problem. Indeed, since

$$\begin{aligned} 2\int_{\mathbf{a}^+}\frac{d\xi}{p^{1/2}(\xi)}&=\oint_{\mathbf{a}}\frac{d\xi}{u(\xi)}=\mathcal{A},\quad \operatorname{Re}\mathcal{A}=0,\\ \oint_{\mathbf{b}}\frac{d\xi}{u(\xi)}&=\mathcal{B},\quad \operatorname{Im}\mathcal{B}=0, \end{aligned} \tag{4.20}$$

and the left-hand side in (4.19) is pure imaginary, we have the following complex equation

$$\int_0^{\boldsymbol{\zeta}_0}\frac{d\xi}{u(\xi)}+n_a\mathcal{A}+n_b\mathcal{B}=g_0, \tag{4.21}$$

where

$$g_0=\frac{1}{4}\int_{dab}\frac{d\xi}{p^{1/2}(\xi)}+\int_0^{\eta_0}\frac{d\xi}{p^{1/2}(\xi)}. \tag{4.22}$$

This is the classical genus-1 Jacobi inversion problem. Notice that the imaginary part of this equation coincides with the condition (4.19) which guarantees the boundedness of the function $X(\zeta,u)$ at infinity. The integrals in (4.20) are the $\mathcal{A}$- and $\mathcal{B}$- periods of the abelian integral in the left-hand side in (4.21) and can be expressed through the Legendre complete elliptic integrals [21]

$$\begin{aligned} \mathcal{A}&=-2i\int_m^{\infty}\frac{d\xi}{\sqrt{|\xi(\xi-1)(\xi-m)|}}=-4ik\mathbf{K}(k),\\ \mathcal{B}&=2\int_1^{m}\frac{d\xi}{\sqrt{|\xi(\xi-1)(\xi-m)|}}=4k\mathbf{K}'(k). \end{aligned} \tag{4.23}$$

Here $k=m^{-1/2}$. To solve the problem (4.21), we make the substitution $\zeta=\tau^2$ and notice that

$$p^{1/2}(\zeta)=-\frac{i\tau}{k}p_0^{1/2}(\tau),\quad p_0^{1/2}(\tau)=\left[\left(1-\tau^2\right)\left(1-k^2\tau^2\right)\right]^{1/2}, \tag{4.24}$$

where the function $p_0^{1/2}(\tau)$ is single-valued in the τ-plane cut along the segments $[-1,1]$ and the segment joining the points $\pm1/k$ and passing through the infinite point. The branch of the function is fixed by the condition $p_0^{1/2}(0^+)=1$.

Assume first that $\boldsymbol{\zeta}_0\in\mathbb{C}_1$. The Jacobi inversion problem becomes then

$$\int_0^{\sqrt{\zeta_0}}\frac{d\tau}{p_0^{1/2}(\tau)}=2n_a\mathbf{K}+2n_bi\mathbf{K}'-\frac{ig_0}{2k}, \tag{4.25}$$

where $\sqrt{\zeta_0}$ is the value of an arbitrary fixed branch of the function $\zeta^{1/2}$ at $\zeta = \zeta_0$. This immediately defines

$$\sqrt{\zeta_0} = -(-1)^{n_a} \operatorname{sn} \frac{ig_0}{2k}, \quad \zeta_0 = \operatorname{sn}^2 \frac{ig_0}{2k}. \tag{4.26}$$

Since the affix ζ_0 is fixed we can evaluate

$$I_\pm = \frac{1}{4} \int_{dab} \frac{d\xi}{p^{1/2}(\xi)} + \int_0^{\eta_0} \frac{d\xi}{p^{1/2}(\xi)} \pm \int_0^{\zeta_0} \frac{d\xi}{p^{1/2}(\xi)}, \tag{4.27}$$

and from (4.25) find the numbers n_a and n_b,

$$n_a = -\frac{\operatorname{Im} I_-}{4k\mathbf{K}}, \quad n_b = \frac{\operatorname{Re} I_-}{4k\mathbf{K}'}. \tag{4.28}$$

If both the numbers are integers, then the problem is solved, and the point $\boldsymbol{\zeta}_0$ lies on the upper sheet. Otherwise, it falls on the lower sheet. In this case, similarly, we get

$$\zeta_0 = \operatorname{sn}^2 \frac{ig_0}{2k}, \quad n_a = -\frac{\operatorname{Im} I_+}{4k\mathbf{K}}, \quad n_b = \frac{\operatorname{Re} I_+}{4k\mathbf{K}'}. \tag{4.29}$$

4.3. Solution to the Riemann–Hilbert problem. Having the solution to the Jacobi inversion problem we are now equipped with a bounded at infinity solution of the factorization problem (4.11). With it, we can represent the term $g(\xi, v)[X^+(\xi, v)]^{-1}$ as

$$\Psi^+(\xi, v) - \Psi^-(\xi, v) = \frac{g(\xi, v)}{X^+(\xi, v)}, \quad (\xi, v) \in l_0 \subset \mathcal{R}, \tag{4.30}$$

By the Sokhotski–Plemelj formulas, the function $\Psi(\zeta, u)$ has the form

$$\begin{aligned} \Psi(\zeta, u) = &-\frac{\alpha}{2\pi i} \int_{ab} \frac{(1 + u/v)d\xi}{X^+(\xi, v)(\xi - \zeta)} \\ &+\frac{\pi - \beta}{2\pi i} \int_{da} \frac{(1 + u/v)d\xi}{X^+(\xi, v)(\xi - \zeta)} - \frac{\sigma'}{2\pi} \int_{bcd} \frac{(1 + u/v)d\xi}{X(\xi, v)(\xi - \zeta)}. \end{aligned} \tag{4.31}$$

Clearly, the function $X(\zeta, u)\Psi(\zeta, u)$ satisfies the Riemann–Hilbert boundary condition (4.9). The general solution can be written as follows:

$$\Phi(\zeta, u) = X(\zeta, u)[\Psi(\zeta, u) + \Omega(\zeta, u)], \tag{4.32}$$

where $\Omega(\zeta, u)$ is a rational function on the surface $\mathcal{R}$. To define this function, we sum up the properties of the functions in (4.32).

(i) Because of the simple pole of the function $\Phi(\zeta, u)$ at the point $\zeta = c$, the function $\Omega(\zeta, u)$ must have a simple pole at the point $\zeta = c$ and be bounded at the point $\zeta = \bar{c} = a$. Then since the function $\Psi(\zeta, u)$ has a logarithmic singularity at the point $\zeta = a$, the same property is valid for the solution to the Riemann–Hilbert problem (4.9) as it is required.

(ii) The function $X(\zeta, u)$ has a simple zero at the point $\boldsymbol{\eta}_0$. Therefore, the function $\Omega(\zeta, u)$ has to have a simple pole at the point $\boldsymbol{\eta}_0$.

(iii) The function $X(\zeta, u)$ has a simple pole at the point $\boldsymbol{\zeta}_0$. Therefore, the function $\Psi(\zeta, u) + \Omega(\zeta, u)$ has to have a simple zero at the point $\boldsymbol{\zeta}_0$.

(iv) The function $X(\zeta,u)$ has a square-root singularity at the point $\zeta=d$. Thus, the function $\Psi(\zeta,u)+\Omega(\zeta,u)$ has to have a simple zero at the point $\zeta=d$.

(v) The function $\Phi(\zeta,u)$ vanishes as $\zeta=\infty$.

(vi) The function $\Phi(\zeta,u)$ must be symmetric; $\Phi(\zeta,u)=\overline{\Phi(\zeta_*,u_*)}$.

The general form of the function $\Omega(\zeta,u)$ which meets the conditions (i), (ii), and (vi) is given by

$$\begin{aligned}\Omega(\zeta,u)=iM_0\frac{u(\zeta)+u(c)}{\zeta-c}+(M_1+iM_2)\frac{u(\zeta)+u(\eta_0)}{\zeta-\eta_0}\\ -(M_1-iM_2)\frac{u(\zeta)-\overline{u(\eta_0)}}{\zeta-\bar\eta_0},\end{aligned}\tag{4.33}$$

where M_j $(j=0,1,2)$ are real constants to be fixed. It is directly verified that the function $\Psi(\zeta,u)$ is symmetric, and the condition (vi) is also met by the function $\Phi(\zeta,u)$. To satisfy the conditions (iii) and (iv) we put

$$\begin{aligned}\Psi(\zeta_0,u(\zeta_0))+\Omega(\zeta_0,u(\zeta_0))=0,\\ \Psi(d,u(d))+\Omega(d,u(d))=0.\end{aligned}\tag{4.34}$$

We emphasize that the former relation is a complex equation while the last one is a real equation. Next, we derive the principal term of the expansion of the function $\Phi(\zeta,u)$ at infinity. Using the condition (v) we find

$$M_0=\Psi_0-2M_2,\tag{4.35}$$

where Ψ_0 is real and

$$\Psi_0=\frac{\alpha}{2\pi}\int_{ab}\frac{d\xi}{vX^+(\xi,v)}-\frac{\pi-\beta}{2\pi}\int_{da}\frac{d\xi}{vX^+(\xi,v)}+\frac{i\sigma'}{2\pi}\int_{bcd}\frac{d\xi}{vX(\xi,v)}.\tag{4.36}$$

We now determine the real constants M_1 and M_2 and the yaw angle δ. Let

$$\rho_0(\zeta)=\frac{u(\zeta)+u(\eta_0)}{\zeta-\eta_0},\quad \rho_1(\zeta)=\frac{u(\zeta)-\overline{u(\eta_0)}}{\zeta-\bar\eta_0},\quad \rho_2(\zeta)=\frac{u(\zeta)+u(c)}{\zeta-c},$$

$$\Psi_1=\Psi(\zeta_0,u(\zeta_0)),\quad \Psi_2=\Psi(d,u(d)).\tag{4.37}$$

Since the position of the wedge is described by the angles $\alpha=\alpha_0+\delta$ and $\beta=\beta_0+\delta$, it will be convenient to represent the constants M_j and Ψ_j $(j=0,1,2)$ in the form

$$M_j=M_j^0+\delta M_j^1,\quad \Psi_j=\Psi_j^0+\delta\Psi_j^1,\tag{4.38}$$

where $\Psi_j^0=\Psi_j|_{\alpha=\alpha_0,\beta=\beta_0}$, and the constants Ψ_j^1 coincide with Ψ_j if α and $\pi-\beta$ are replaced by 1 and -1, respectively. On using (4.34), it is a matter of simple algebra to show that

$$\begin{aligned}M_1^\nu&=\frac{1}{\Delta}\left\{[\Psi_0^\nu\operatorname{Im}\rho_2(\zeta_0)-\operatorname{Re}\Psi_1^\nu]\operatorname{Re}\mu_1-[\Psi_0^\nu\operatorname{Re}\rho_2(\zeta_0)+\operatorname{Im}\Psi_1^\nu]\operatorname{Im}\mu_1\right\},\\ M_2^\nu&=-\frac{1}{\Delta}\left\{[\Psi_0^\nu\operatorname{Re}\rho_2(\zeta_0)+\operatorname{Im}\Psi_1^\nu]\operatorname{Re}\mu_2+[\Psi_0^\nu\operatorname{Im}\rho_2(\zeta_0)-\operatorname{Re}\Psi_1^\nu]\operatorname{Im}\mu_2\right\},\quad \nu=0,1,\\ \delta&=-\frac{\Delta_0}{\Delta_1},\end{aligned}\tag{4.39}$$

where

$$\Delta = \operatorname{Re}\mu_1 \operatorname{Re}\mu_2 + \operatorname{Im}\mu_1 \operatorname{Im}\mu_2,$$
$$\mu_1 = \rho_0(\zeta_0) + \rho_1(\zeta_0) - 2\rho_2(\zeta_0), \quad \mu_2 = \rho_0(\zeta_0) - \rho_1(\zeta_0),$$
$$\Delta_\nu = \Psi_2^\nu + i\rho_2(d)M_0^\nu + [\rho_0(d) - \rho_1(d)]M_1^\nu + i[\rho_0(d) + \rho_1(d)]M_2^\nu, \quad \nu = 0, 1. \tag{4.40}$$

Analysis of the right-hand side in the third formula in (4.39) shows that it is real.

5. Numerical results.

5.1. Parameters a, b, d, and m. In the preceding sections, the expression of the derivative $df/d\zeta$ of the conformal mapping $z = f(\zeta)$ was obtained by formula (2.6) in terms of the functions $\omega_0(\zeta)$ and $\omega_1(\zeta) = i\Phi(\zeta, u)$, $(\zeta, u) \in \mathbb{C}_1$ defined by (3.3) and (4.32), respectively. There are four parameters, a, b, d, and m, left to be fixed. In general, the conformal mapping found does not satisfy the single-valuedness condition

$$\int_{L_1^*} dz = 0, \tag{5.1}$$

and the points a, b, and d of the parametric domain are not necessarily the images of the points A, B, and D, respectively. Here L_1^* is a closed contour in the flow domain such that $L_1^* \supset L_1$. To ensure this we require

$$\int_{l_1^*} \tilde{\omega}_0(\zeta) e^{-\omega_1(\zeta)} d\zeta = 0,$$
$$\lambda_1 \sin\alpha - N\Omega_1 = 0,$$
$$\lambda_2 \sin\beta - N\Omega_2 = 0, \tag{5.2}$$

where

$$\Omega_1 = \operatorname{Im}\int_{ab} \tilde{\omega}_0(\zeta) e^{-\omega_1(\zeta)} d\zeta, \qquad \Omega_2 = \operatorname{Im}\int_{da} \tilde{\omega}_0(\zeta) e^{-\omega_1(\zeta)} d\zeta, \tag{5.3}$$

and l_1^* is a closed contour which does not cross the cut l_0 and $l_1^* \supset l_1$. For numerical purposes, l_1^* can be chosen as follows:

$$l_1^* = \left\{ \zeta : \left| \zeta - \frac{1}{2} \right| = r^* \right\}, \qquad \frac{1}{2} < r^* < m - \frac{1}{2}. \tag{5.4}$$

The first equation in (5.2) is complex, and the other two are real. Thus, equations (5.2) constitute a system of four real nonlinear equations for the unknown parameters a, b, d, and m. Without loss of generality we may accept that $a \in l_1^+$. Then $c = \bar{a} \in l_1^-$, $a < b < 1$, and $0 < d < a$. Based on the results [2] for a supercavitating wedge in a plane, we assume that $b \in l_1^+$ and $d \in l_1^+$. For all the parameters of the problem chosen for the tests, this assumption is confirmed numerically. The unknown parameters a, b, d, and m have to meet the following constraints: $0 < d < a < b < 1$ and $m > 1$. To eliminate the constraints we introduce a new vector $\mathbf{x} = \{x_0, x_1, x_2, x_3\}$ [25] whose components are

$$x_0 = \ln(m-1), \quad x_1 = \ln\frac{d}{a-d}, \quad x_2 = \ln\frac{a-d}{b-a}, \quad x_3 = \ln\frac{b-a}{1-b},$$
$$-\infty < x_j < +\infty, \quad j = 0, 1, 2, 3. \tag{5.5}$$

TABLE 1

The values of the parameters a, b, d, m, and the yaw angle δ in the case (5.9) *for some values of depth h.*

h	a	b	d	$m-1$	δ
100	0.530751	0.676380	0.379709	1.566769	$0.469847 \cdot 10^{-4}$
75	0.540767	0.685701	0.388635	1.078599	0.000109
50	0.560192	0.703909	0.405768	0.605359	0.000353
25	0.611911	0.753061	0.450134	0.181660	0.002286
10	0.710496	0.847700	0.528498	$0.182847 \cdot 10^{-1}$	0.016236
5	0.783349	0.915387	0.576899	$0.138606 \cdot 10^{-2}$	0.04620
4	0.803352	0.932955	0.587015	$0.488768 \cdot 10^{-3}$	0.060882
3	0.829184	0.952958	0.601417	$0.106904 \cdot 10^{-3}$	0.082173
2	0.824997	0.967054	0.528133	$0.619607 \cdot 10^{-5}$	0.146737
1.5	0.820221	0.969388	0.500073	$0.238153 \cdot 10^{-5}$	0.165417

The nonlinear system (5.2) written in the form $\mathbf{r}(\mathbf{x}) = 0$ for the new unknown parameters is solved by the Newton method

$$\mathbf{x}^{(n+1)} = \mathbf{x}^{(n)} - \left[F\left(\mathbf{x}^{(n)}\right)\right]^{-1} \mathbf{r}\left(\mathbf{x}^{(n)}\right), \quad n = 0, 1, \ldots, \tag{5.6}$$

where $[F(\mathbf{x})]^{-1}$ is the inverse of the Jacobian matrix $F = (\partial r_i/\partial x_j)$, $i, j = 0, \ldots, 3$, evaluated approximately

$$\frac{\partial r_i}{\partial x_j} \approx \frac{r_i(x_0, \ldots, x_j + \delta x_j, \ldots, x_3) - r_i(x_0, \ldots, x_j, \ldots, x_3)}{\delta x_j}. \tag{5.7}$$

The parameters of the conformal mapping are recovered through the solution to the system $\mathbf{r}(\mathbf{x}) = 0$ by the formulas

$$m = 1 + e^{x_0}, \quad a = \frac{x_2^* x_3^* (1 + x_1^*)}{\Delta^*}, \quad b = \frac{x_3^* (1 + x_2^* + x_1^* x_2^*)}{\Delta^*}, \quad d = \frac{x_1^* x_2^* x_3^*}{\Delta^*},$$

$$\Delta^* = 1 + x_3^* (1 + x_2^* + x_1^* x_2^*), \quad x_j^* = e^{x_j}, \quad j = 1, 2, 3. \tag{5.8}$$

The idea to work with the variables x_j, not with the original unknowns a, b, d, and m, is fruitful for two reasons. First, we get rid of the constraints and can apply the classical Newton scheme, and, second, the variations of an approximate solution $\mathbf{x}^{(n)}$ in a neighborhood of the exact solution $\mathbf{x}$ are bigger than the variations of the corresponding approximate values of the parameters a, b, d, and m.

Computations implemented for the parameters

$$\alpha_0 = \frac{\pi}{3}, \quad \beta_0 = \frac{2\pi}{3}, \quad \lambda_1 = 1, \quad \lambda_2 = 1, \quad \sigma = 0.5, \tag{5.9}$$

and for different values of the depth h show that indeed $a, b, d \in l_1^+ (c = \bar{a} \in l_1^-)$. The effect of the free boundary on the location of the parameters of the conformal mapping is substantial even for big depths (Table 1).

For the parameters chosen it is found that $a \to 0.5$, $b \to 0.64848$, $d \to 1 - b$, $m \to \infty$, and $\delta \to 0$ when $h \to \infty$. This is consistent with the corresponding result

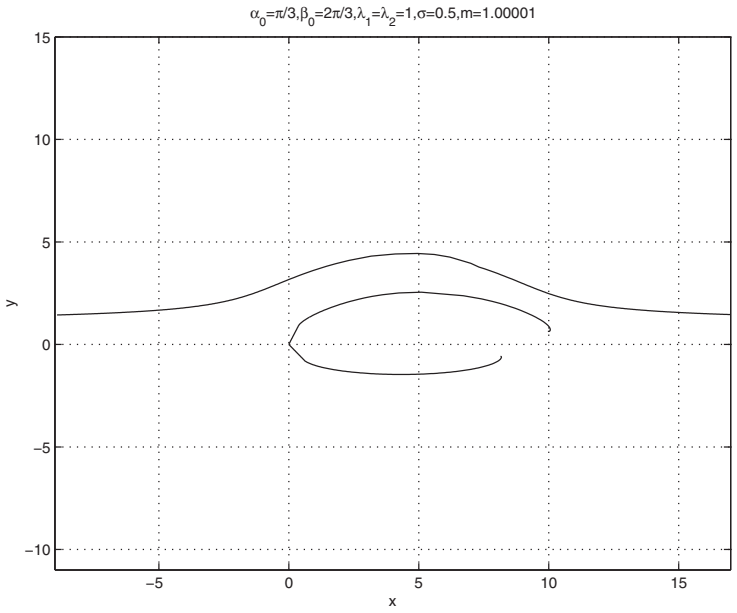

FIG. 3. *The cavity shape and the free surface for* $\alpha_0 = \frac{\pi}{3}$, $\beta_0 = \frac{2\pi}{3}$, $\lambda_1 = \lambda_2 = 1$, $\sigma = 0.5$, *and* $h = 2.11527$.

for a wedge in a plane [2]. When h is decreasing, then, first, the four parameters, a, b, c, and d are moving to the right. But then, for small h, the parameters a, c, and d are moving back while the parameter b continues approaching the branch point $\zeta = 1$ of the surface. As for the parameter m, when h is increasing it grows as well. However, the rate of growth is different. It turns out that when the wedge is close to the free surface and the depth is in the range $h \in (1.5, 4)$, the parameter $m - 1$ is very small: $m - 1 \in (0.2 \cdot 10^{-5}, 0.5 \cdot 10^{-3})$. Also, when a symmetric wedge is approaching the free surface, the angle of yaw δ is increasing and becomes noticeable for small h (Table 1).

5.2. Cavity shape, the free surface, drag, lift, and the circulation. To restore the shape of the cavity, we integrate the function $df/d\zeta$ over the contours $b\tau$ ($\tau \in bc$) and $d\tau$ ($\tau \in dc$) to obtain the upper and lower boundaries, respectively,

$$z(\tau) = B + \int_{b\tau} \frac{df}{d\zeta} d\zeta, \ \tau \in bc \ (z \in BC^+),$$

$$z(\tau) = D + \int_{d\tau} \frac{df}{d\zeta} d\zeta, \ \tau \in dc \ (z \in DC^-). \tag{5.10}$$

Similarly, for the free surface,

$$z(\tau) = B + \int_{b\tau} \frac{df}{d\zeta} d\zeta, \ \tau \in l_0 \ (z \in E^- E^+). \tag{5.11}$$

Figure 3 shows the cavity shape and the free boundary for the parameters (5.9) when $m = 1.00001$. In this case $h = 2.11527$, $a = \overline{c} = 0.83010$, $b = 0.96627$, and $d = 0.54931$. It is seen that the presence of the free boundary breaks the symmetry of the cavity. On the other hand, the supercavitating wedge creates waves on the free surface. Their amplitude becomes higher when the wedge approaches the boundary

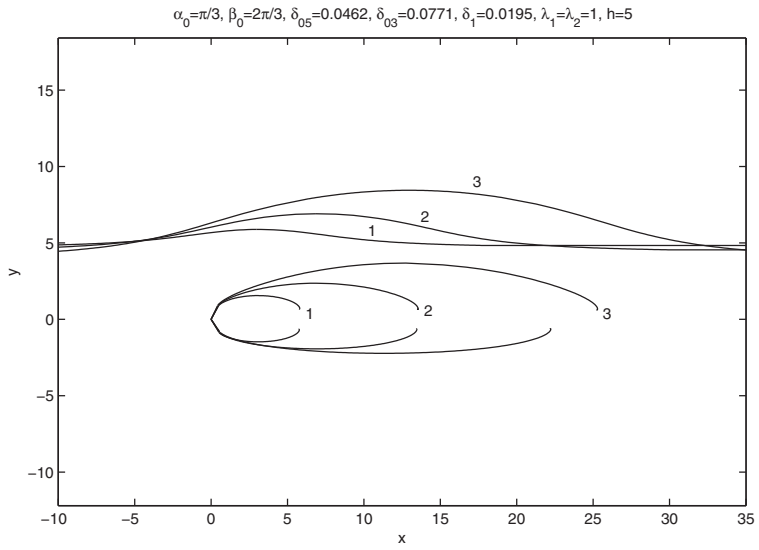

FIG. 4. *The cavity shape and the free surface when* $\alpha_0 = \frac{\pi}{3}$, $\beta_0 = \frac{2\pi}{3}$, $\lambda_1 = \lambda_2 = 1$, *and* $h = 5$ *for some values of the cavitation number* σ*:* $\sigma = 1$ (1), $\sigma = 0.5$ (2), *and* $\sigma = 0.3$ (3).

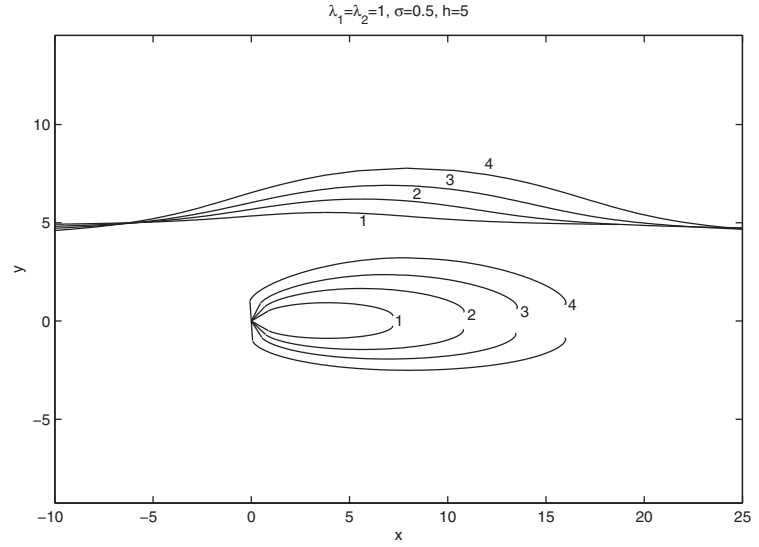

FIG. 5. *The cavity shape and the free surface when* $\lambda_1 = \lambda_2 = 1$, $h = 5$, *and* $\sigma = 0.5$ *for some values of the angle* α_0*:* $\alpha_0 = \frac{\pi}{6}$ (1), $\alpha_0 = \frac{\pi}{4}$ (2), $\alpha_0 = \frac{\pi}{3}$ (3), *and* $\alpha_0 = \frac{\pi}{2}$ (4) ($\beta_0 = \pi - \alpha_0$).

(Figure 3 and Figure 4) or when the cavitation number decreases (Figure 4). It is found that for big depths, the cavity is practically symmetric as it should be [2]. When h is decreasing, the corresponding parameters b, $a = \bar{c}$, and d are moving to the left end of the segment $[0, 1]$. After h has passed a certain critical point, and the wedge is close enough to the free surface, the parameter d is moving back to the left. The cavity grows and the yaw angle increases when the cavitation number σ decreases.

We have also computed the solution for different angles α_0 ($\beta_0 = \pi - \alpha_0$) (Figure 5). It turns out that the cavity and the amplitude of the waves on the free surface

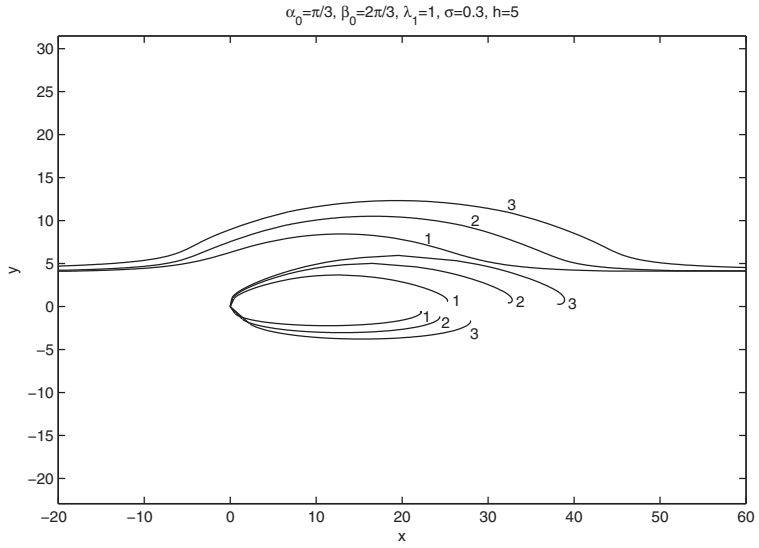

FIG. 6. *The cavity shape and the free surface for a nonsymmetric wedge when* $\alpha_0 = \frac{\pi}{3}$, $\beta_0 = \frac{2\pi}{3}$, $\sigma = 0.3$, $h = 5$, *and* $\lambda_1 = 1$ *for some values of* λ_2*:* $\lambda_2 = 1$ (1), $\lambda_2 = 2$ (2), *and* $\lambda_2 = 3$ (3).

grow when the angle α_0 grows. The length of the cavity and the amplitude of the waves attain their maximum for $\alpha_0 = \frac{\pi}{2}$, for a hydrofoil orthogonal to the free surface at rest. The same tendency is observed for the yaw angle: $\delta = 0.0106$ for $\alpha_0 = \frac{\pi}{6}$, $\delta = 0.0284$ for $\alpha_0 = \frac{\pi}{4}$, $\delta = 0.0462$ for $\alpha_0 = \frac{\pi}{3}$, and $\delta = 0.0665$ for $\alpha_0 = \frac{\pi}{2}$.

In Figure 6, the cavity shape and the free surface for the symmetric wedge $\lambda_1 = \lambda_2 = 1$ are compared with the corresponding profiles for two nonsymmetric wedges, $\lambda_2 = 2$ and $\lambda_2 = 3$, while $\lambda_1 = 1$.

Figure 7 shows the effect on the length, l_c, of the upper and lower boundaries of the cavity of changing the depth h. It is seen that when the wedge approaches the surface both the lengths decrease. The upper boundary becomes longer than the lower one for small depths.

The spiral shape of the cavity at a neighborhood of the upper lower vortices C^+ and C^- is shown in Figs. 8(a) and 8(c), respectively. A closer neighborhood of the same points is given in Figs. 8(c) and 8(d). By approaching the lower vortex C^-, the spiral structure of the cavity becomes evident (Figure 9).

To clarify how the flow behaves near the centers of the vortices, we plot the upper branch of the streamlines $\psi(x, y) = C_0$, $C_0 = hV_0/20$ (1), $hV_0/50$ (2), $hV_0/100$ (3), $hV_0/1000$ (4), and $hV_0/10000$ (5) close to the streamline $\psi(x, y) = 0$ (6) which defines the cavity boundary (Figure 10). The preimages of these streamlines are shown in Figure 11. It is seen that the preimage of the streamline $\psi = 0$ is orthogonal to the slit $[0, 1]$ while the others are not. For small values of the constant C_0, the streamline $\psi(x, y) = C_0$ first spirals and then proceeds to sheets of the Riemann surface of a logarithmic function with the branch points C^+ and C^-. The number of sheets used for modeling the flow is infinite for $C_0 = 0$ and decreases as C_0 increases. For example, for $C_0 = hV_0/100$ (line 3 in Figure 10), the flow does not leave the physical plane.

Next we determine the drag, X, and the lift, Y, by

$$X + iY = -i \int_{DAB} (p - p_1) dz, \tag{5.12}$$

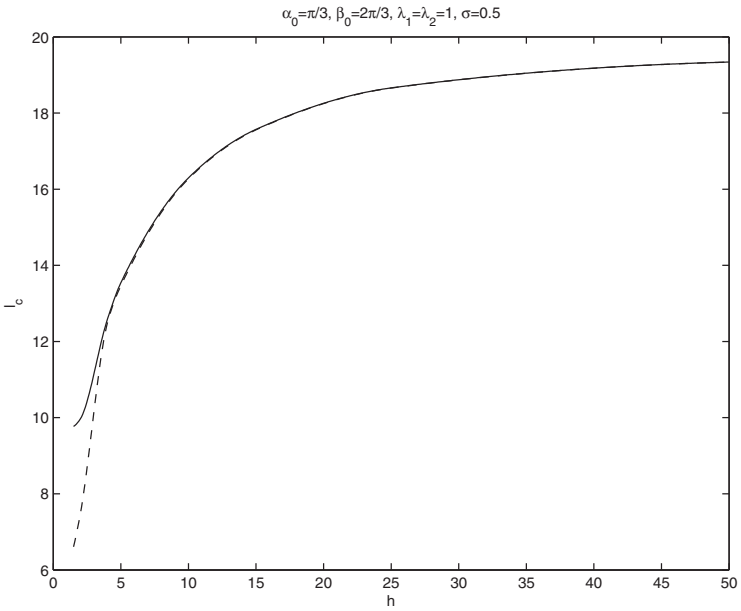

FIG. 7. *The length of the upper (the solid line) and lower (the broken line) boundaries of the cavity versus the depth* h *when* $\alpha_0 = \frac{\pi}{3}$, $\beta_0 = \frac{2\pi}{3}$, $\lambda_1 = \lambda_2 = 1$, *and* $\sigma = 0.5$.

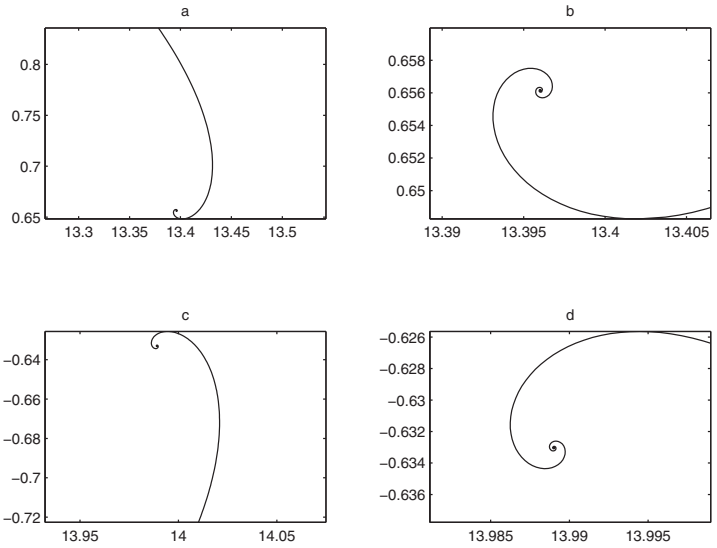

FIG. 8. *The cavity shape in the vicinity of the upper* (a, b) *and the lower* (c, d) *vortices* ($\alpha_0 = \frac{\pi}{3}$, $\beta_0 = \frac{2\pi}{3}$, $\lambda_1 = 1$, $\lambda_2 = 1$, $\sigma = 0.5$, *and* $h = 5$).

where p is the water pressure in $\tilde{\mathcal{D}}$ and p_1 is the vapor pressure in the cavity. By using the Bernoulli law, $p - p_1 = \frac{1}{2}\rho(V_1^2 - V^2)$, $V = |\mathbf{v}|$, and since

$$V^2 = V_0^2 e^{2\,\mathrm{Re}\,\omega_1(\zeta)}, \tag{5.13}$$

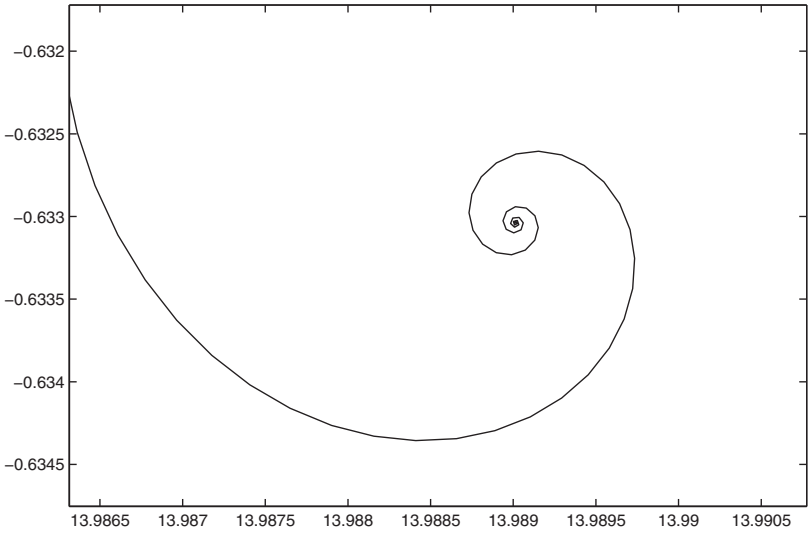

FIG. 9. *The cavity shape in the vicinity of the lower vortex C^-: a closer look* ($\alpha_0 = \frac{\pi}{3}$, $\beta_0 = \frac{2\pi}{3}$, $\lambda_1 = 1$, $\lambda_2 = 1$, $\sigma = 0.5$, *and* $h = 5$).

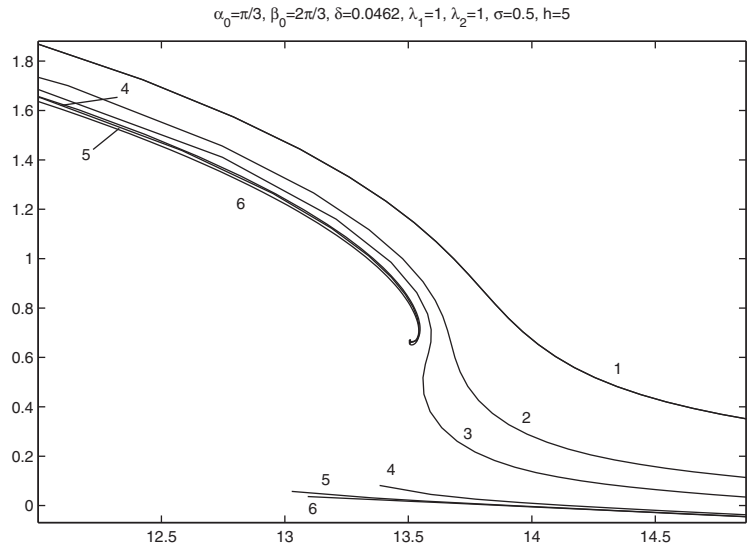

FIG. 10. *The streamlines $\psi(x, y) = hV_0/I$ close to the center of the upper vortex when* $\alpha_0 = \frac{\pi}{3}$, $\beta_0 = \frac{2\pi}{3}$, $\lambda_1 = 1$, $\lambda_2 = 1$, $h = 5$, $V_0 = 1$, *and* $\sigma = 0.5$*: $I = 20$ (1), $I = 50$ (2), $I = 100$ (3), $I = 1000$ (4), $I = 10000$ (5), and $I = \infty$ (6).*

we obtain

$$X + iY = -\frac{i\rho}{2} \int_{dab} \left(V_1^2 - V_0^2 e^{2\,\mathrm{Re}\,\omega_1(\zeta)} \right) e^{-\omega_1(\zeta)} \omega_0(\zeta) d\zeta. \tag{5.14}$$

The drag and lift coefficients, C_X and C_Y, related to the velocity at infinity V_0 and

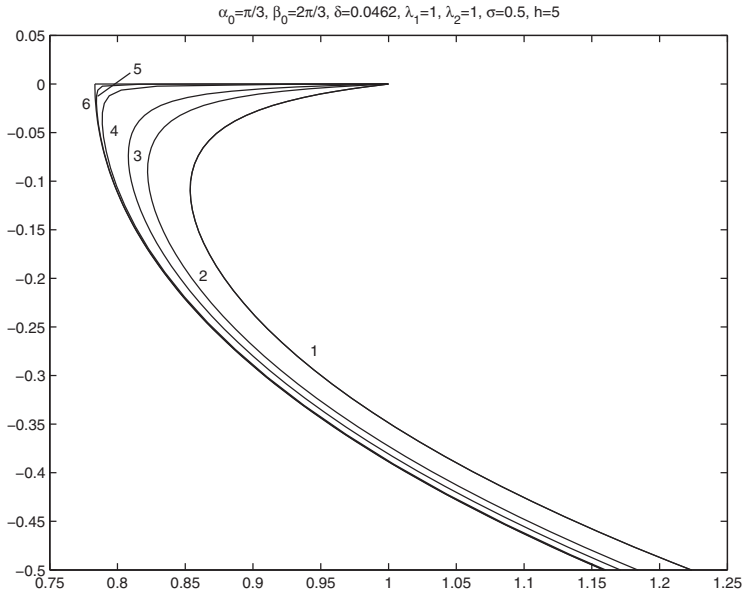

FIG. 11. *The preimages of the streamlines* $\psi(x,y) = hV_0/I$ *close to the center of the upper vortex when* $\alpha_0 = \frac{\pi}{3}$, $\beta_0 = \frac{2\pi}{3}$, $\lambda_1 = 1$, $\lambda_2 = 1$, $h = 5$, $V_0 = 1$, *and* $\sigma = 0.5$*:* $I = 20$ (1), $I = 50$ (2), $I = 100$ (3), $I = 1000$ (4), $I = 10000$ (5), *and* $I = \infty$ (6).

TABLE 2

The values of the drag and lift coefficients, C_X *and* C_Y*, and the circulation* Γ *in the case* (5.9) *for some values of depth* h*.*

h	C_X	C_Y	Γ
200	2.043086	−0.004891	−0.003292
100	2.012256	−0.004823	−0.004020
75	2.004884	−0.004707	−0.004202
50	1.998008	−0.004248	−0.006300
25	1.992799	−0.000513	−0.025780
10	1.991986	0.026710	−0.325814
5	1.987338	0.098340	−1.225218
4	1.983682	0.114038	−1.404919
3	1.975224	0.15548	−2.204043
2	1.947963	0.279897	−3.510621
1.5	1.938851	0.315563	−3.571451

the length $\lambda = \lambda_1 \sin\alpha + \lambda_2 \sin\beta$, are

$$C_X + iC_Y = \frac{2}{\rho V_0^2 \lambda}(X + iY). \tag{5.15}$$

These coefficients can be computed by the formula

$$C_X + iC_Y = -\frac{i}{\lambda}\int_{dab}\left[\sigma + 1 - e^{2\,\mathrm{Re}\,\omega_1(\zeta)}\right] e^{-\omega_1(\zeta)}\omega_0(\zeta)d\zeta. \tag{5.16}$$

Table 2 shows the effect on the drag and lift coefficients of varying the depth h. It is seen that the drag coefficient is decreasing and the lift coefficient is increasing when the wedge is approaching the free boundary.

TABLE 3

The values of the coefficients C_X, C_Y, and C_n in the case (5.9) when $h = 5$ for some values of the cavitation number σ.

σ	0.175	0.2	0.25	0.3	0.4	0.5	0.6	0.7	0.8	0.9	1.0
C_X	1.513	1.545	1.598	1.707	1.815	1.987	2.089	2.237	2.372	2.521	2.699
C_Y	0.114	0.124	0.154	0.123	0.113	0.098	0.088	0.083	0.075	0.071	0.067
C_n	1.518	1.550	1.605	1.711	1.819	1.990	2.094	2.239	2.373	2.553	2.700

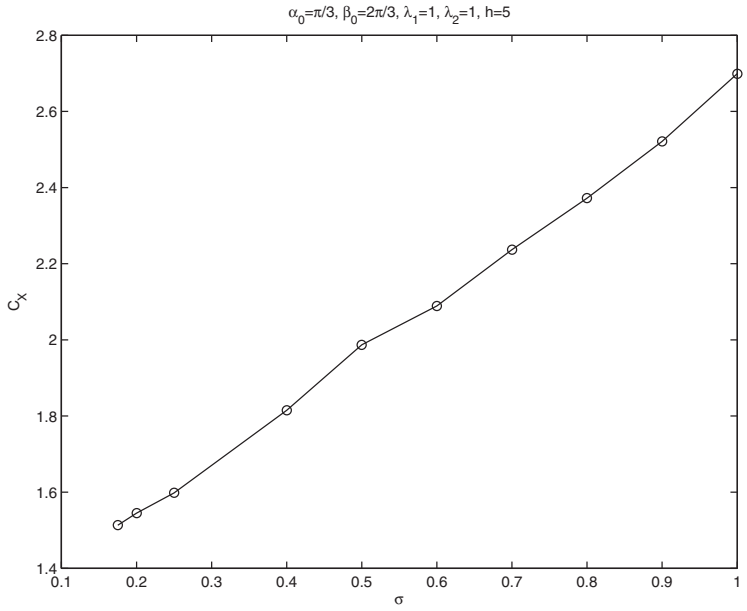

FIG. 12. *The drag coefficient versus the cavitation number σ for $\alpha_0 = \frac{\pi}{3}$, $\beta_0 = \frac{2\pi}{3}$, $\lambda_1 = 1$, $\lambda_2 = 1$, and $h = 5$.*

Figures 12 and 13 show the effect on the drag and lift coefficients of changing the cavitation number. It is seen that the drag coefficient is a linearly increasing function of the cavitation number σ while lift first increases, attains its maximum, and then decreases. The variation of the lift coefficient is small in comparison with that of the drag coefficient, and the value $C_n = \sqrt{C_X^2 + C_Y^2}$ monotonically increases (see Table 3) as it does for a supercavitating plate in a plane [16].

Next, we determine the circulation of the velocity around the closed contour $L_1 = ABCDA$,

$$\Gamma = \int_{l_1^*} \frac{dw}{d\zeta} d\zeta = NV_0 \int_{l_1^*} \tilde{\omega}_0(\zeta) d\zeta, \tag{5.17}$$

where l_1^* is the preimage of the contour L_1. In Table 2, we present the values of the circulation Γ/V_0 for some values of the depth h.

Finally, we compute the singularity factor K in the Terent'ev formula (2.5),

$$K = -\lim_{\zeta \to c} \omega_1(\zeta)[w(z) - w(C)]^{1/2}. \tag{5.18}$$

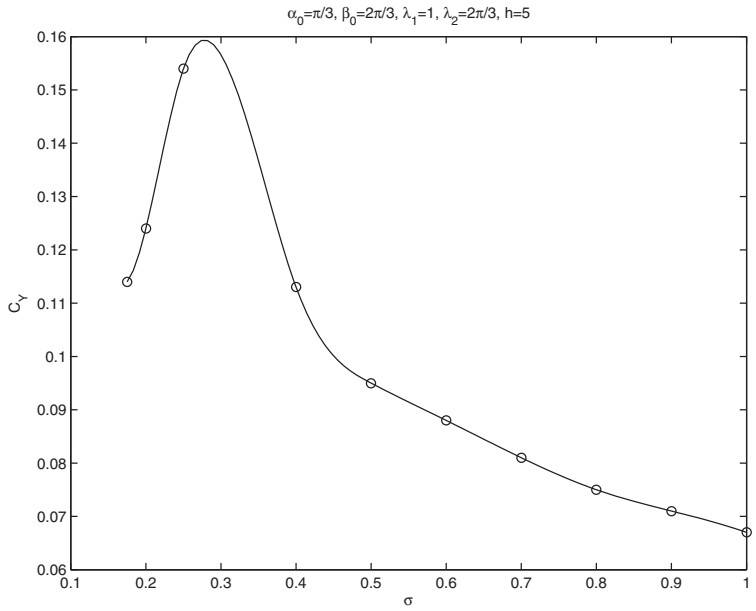

FIG. 13. *The lift coefficient versus the cavitation number* σ *for* $\alpha_0 = \frac{\pi}{3}$, $\beta_0 = \frac{2\pi}{3}$, $\lambda_1 = 1$, $\lambda_2 = 1$, *and* $h = 5$.

Since

$$\left.\frac{dw}{d\zeta}\right|_{\zeta=c} = 0, \quad \left.\frac{d^2w}{d\zeta^2}\right|_{\zeta=c} = \frac{V_0 N}{\sqrt{|p(c)|}}, \tag{5.19}$$

by expanding the function $w(z(\zeta))$ in a Taylor series, we obtain

$$w(z) - w(C) \sim \frac{V_0 N}{2\sqrt{|p(c)|}}(\zeta - c)^2, \quad z \to C \quad (\zeta \to c). \tag{5.20}$$

Numerical results for different data show that $N < 0$. Because of the chosen branch of the function $[w(z) - w(C)]^{1/2}$, we have $\arg[-(\zeta - c)^2] \in [-\pi, \pi]$. Now, $\arg(\zeta - c) \in [-\pi, 0]$, and therefore, $[N(\zeta - c)^2]^{1/2} = i\sqrt{|N|}(\zeta - c)$. This implies

$$[w(z) - w(C)]^{1/2} \sim i\sqrt{\frac{V_0|N|}{2\sqrt{|p(c)|}}}(\zeta - c), \quad \zeta \to c. \tag{5.21}$$

The resulting formula for the factor K comes from (4.32) and (4.33),

$$K = -M_0 \left| X\left(c, p^{1/2}(c)\right)\right| \sqrt{2V_0|N|\sqrt{|p(c)|}}. \tag{5.22}$$

Numerical tests implemented for different values of the parameters of the problem show that this constant is indeed positive. For example, for $V_0 = 1$, $h = 5$, and the data (5.9), we have $K = 0.502650$ ($M_0 = -0.30993$ and $N = -7.32526$). Notice that the other parameters in this case are $a = 0.783349$, $b = 0.915387$, $d = 0.576899$, and $m = 1.00138606$.

5.3. Numerical aspects of the algorithm. In order to recover the mapping parameters, the shape of the cavity, the free surface, and drag and lift, we need to compute some integrals, regular and singular. The first quadratures come from the solution to the factorization problem (4.11). Its solution for $(\zeta, u) \in \mathcal{R} \setminus \mathcal{L}$ is given by formula (4.17), and the boundary value of this function on the contour *bcd* becomes $X^+(\xi, v) = X(\xi, v)$. The first integral in the representation of $X(\xi, v)$ is singular and is understood in the sense of the principal value. To evaluate the exponent of this integral for $\xi \in l_1^+$, it is convenient to transform it into the form

$$\exp\left\{\frac{1}{4}\int_{dab}\left(1+\frac{u(\xi)}{u(\tau)}\right)\frac{d\tau}{\tau-\xi}\right\}$$

$$= \left|\frac{\xi-b}{\xi-d}\right|^{1/2} \exp\left\{\frac{1}{4}\int_{dab}\left(-1+\frac{u(\xi)}{u(\tau)}\right)\frac{d\tau}{\tau-\xi}\right\}, \quad \xi \in l_1^+, \quad dab \subset l_1^+. \tag{5.23}$$

The integral in the right-hand side is regular. This quadrature, as the other integrals in the representation of the function $X(\zeta, u)$, is evaluated by the Gauss quadrature rule.

We recall that the function $X(\zeta, u)$ is bounded at infinity if and only if the point $\boldsymbol{\zeta}_0$ and the integer n_a satisfy the Jacobi inversion problem (4.21) (the function $X(\zeta, u)$ is independent of the second integer n_b). It turns out that for all the parameters α_0, β_0, λ_1, λ_2, σ, and h and the started point $\boldsymbol{\eta}_0 \in \mathbb{C}_1$ we tested, the point $\boldsymbol{\zeta}_0$ always falls in the upper sheet, and $n_a = n_b = 0$. For example, for the parameters (5.9), $h = 5$, and $\boldsymbol{\eta}_0 = (i, p^{1/2}(i))$, the affix of the point $\boldsymbol{\zeta}_0 \in \mathbb{C}_1$ is $\zeta_0 = 0.51516 + i0.85739$.

Double integrals become involved in the representation (4.31) of the function $\Psi(\zeta, u)$ and therefore of the function $\Phi(\zeta)$. The boundary value $\Phi^+(\xi, v)$ is recovered by the Sokhotski–Plemelj formula, and it is given by

$$\Phi^+(\xi, v) = \frac{1}{2}g(\xi, v) + X^+(\xi, v)[\Psi(\xi, v) + \Omega(\xi, v)], \quad (\xi, v) \in l_1. \tag{5.24}$$

The principal values of the singular integrals in (5.24) are computed by using the formula

$$\int_{\delta_1}^{\delta_2} \frac{[1 + u(\xi)/u(\tau)]d\tau}{X^+(\tau, u(\tau))(\tau - \xi)} = \frac{\pi}{n}\sum_{j=1}^{n} H(\tau_j, \xi), \quad \delta_1 < \xi < \delta_2, \tag{5.25}$$

where $\tau_j = \frac{1}{2}(\delta_2 + \delta_1) + \frac{1}{2}(\delta_2 - \delta_1)\cos[(j - \frac{1}{2})\pi/n]$,

$$H(\tau, \xi) = \frac{1}{\tau - \xi}\left[\left(1 + \frac{u(\xi)}{u(\tau)}\right)\frac{\sqrt{(\delta_2 - \tau)(\tau - \delta_1)}}{X^+(\tau, u(\tau))} - \frac{2\sqrt{(\delta_2 - \xi)(\xi - \delta_1)}}{X^+(\xi, u(\xi))}\right]. \tag{5.26}$$

It is derived from the order n Gauss quadrature rule and the fact that the principal value of the Cauchy integral of the function $[(\delta_2 - \tau)(\tau - \delta_1)]^{-1/2}$ over the segment (δ_1, δ_2) is equal to 0.

The formulas (5.2), (5.3), (5.10), and (5.11) require the integration of the function $\omega_0(\zeta)e^{-\omega_1(\zeta)}$. This gives triple integrals. For their evaluation, the Gauss quadrature formulas appear to be efficient. To plot the shape of the cavity and the free surface, it becomes useful to use the following preimages of points on the curves BC, DC, and

E^-E^+:

$$
\begin{aligned}
\xi_j^{++} &= b + (1-b)\sin js_0 \in b1, \quad z \in Bz_B,\\
\xi_j^{+-} &= c + (1-c)\cos js_0 \in 1c, \quad z \in z_BC, \quad j = 1, 2, \ldots, k_0,\\
\xi_j^{--} &= c - c\cos js_1 \in 0c, \quad z \in z_DC,\\
\xi_j^{-+} &= d - d\sin js_1 \in d0, \quad z \in Dz_D, \quad j = 1, 2, \ldots, k_1,\\
\eta_j^{+} &= m + r(1 - \sin js_2) \in e_0^- m \subset l_0^+,\\
\eta_j^{-} &= m + r(1 - \cos js_2) \in me_0^+ \subset l_0^-, \quad j = 1, 2, \ldots, k_2,
\end{aligned} \tag{5.27}
$$

where $r > 0$, $s_i = \pi/(2k_i)$, $i = 0, 1, 2$; $2k_0$, $2k_1$, and $2k_2$ are the numbers of the points taken to reconstruct the curves BC, DC, and E^-E^+, respectively. The points z_B and z_D are the images of the branch points $\zeta = 1$ and $\zeta = 0$ of the surface $\mathcal{R}$, respectively. The points e_0^- and e_0^+ are the preimages of the ending points E_0^- and E_0^+ of a piece of the free boundary E^-E^+ we want to reconstruct.

Conclusions. In this work, a method of conformal mappings has been developed for a model problem on the uniform motion of a supercavitating yawed wedge beneath a free surface. To describe the motion, we have used the Tulin–Terent'ev single-spiral-vortex model. By contrast with the double-spiral-vortex model which would lead to a boundary-value problem for a simply connected domain, the model employed requires studying the motion in a doubly connected domain. We have shown that the derivative of the conformal mapping $df/d\zeta$ from the exterior of two slits, $[0, 1]$ and $[m, \infty)$, in a parametric plane into the flow domain can be expressed through the solutions to two boundary-value problems of the theory of analytic functions. The first problem is a standard Hilbert problem for two segments on a plane. The second one is a Riemann–Hilbert problem on a Riemann (elliptic) surface. We have managed to solve both the problems in a closed form. The formula for $df/d\zeta$ we have derived possesses four unknown parameters. These parameters have been recovered from a system of four nonlinear equations by the Newton method.

We have implemented the method numerically. One of the key steps of the procedure is the solution of the parameter problem. Based on the previous analysis [2] for the case of a wedge in a plane, as the first approximation, we have chosen the parameters b and d to be located on the upper side of the slit $[0, 1]$, the side where the parameter a is placed. Since we have proved that $c = \bar{a}$, this choice allows the points a, b, and d slide along the upper side of the slit and never be on the lower side while the point c is always on the lower side of the slit and $|c| = |a|$. We have also tried the other three possibilities, (i) $b \in [0, 1]^-$, $d \in [0, 1]^-$, (ii) $b \in [0, 1]^-$, $d \in [0, 1]^+$, and (iii) $b \in [0, 1]^+$, $d \in [0, 1]^-$ (while $a = \bar{c} \in [0, 1]^+$). It turns out that for different values of the physical parameters the system of transcendental equations does not have solution in these three cases. Comparing this method with the one that maps a doubly connected circular domain (an annulus or the exterior of two circles) onto the flow domain, we note that the method we have presented derives a closed-form solution and requires the computation of certain singular and regular integrals along some real segments. The method of automorphic functions recently developed for an $n + 1$-connected flow domain and numerically implemented for a simply connected case [3] if applied to the present problem would derive the solution in a series form and would need to compute singular and regular integrals over arcs and their images. It may happen that for triply connected flow domains the unknown parameters can be on any side of the cuts, and then to map the exterior of a circular domain onto the flow domain will be a better approach.

It has been shown that the free surface affects the angle of yaw, the circulation integral, the lift and drag coefficients, and breaks the symmetry of the cavity even if the wedge is symmetric. When the wedge approaches the free surface the angle of yaw, the circulation and the lift increase while the drag decreases. When the wedge approaches the free surface, the upper boundary becomes noticeably longer than the lower one. We have also found that when h decreases to 0 the parameter m decreases to 1. However, the decrease rate for h and m is different. For example, in the case (5.9), for $h = 100$, $h = 10$, and $h = 2$, we have the following values of the parameter m: $m = 2.56677$, $m = 1+0.18285\cdot 10^{-1}$, and $m = 1+0.61961\cdot 10^{-5}$, respectively. The numerical scheme is stable even when m is very close to another branch point $\zeta = 1$. The ability of the present method to deal with small $m - 1$ makes it applicable for wedges moving at small depths (for the data (5.9) the method is stable for $h \geq 1.5$).

This method can also be employed for the Tulin–Terent'ev model for a wedge moving in a jet or a wind tunnel. The analysis of the problem for a wedge in a jet and the comparison of the numerical results produced by the Tulin–Terent'ev single-spiral-vortex model and the Tulin double-spiral-vortex model are the subjects of a future publication.

REFERENCES

[1] Y.A. Antipov and V.V. Silvestrov, *Method of Riemann surfaces in the study of supercavitating flow around two hydrofoils in a channel*, Phys. D, 235 (2007), pp. 72–81.

[2] Y.A. Antipov and V.V. Silvestrov, *Double cavity flow past a wedge*, Proc. R. Soc. A, 464 (2008), pp. 3021–3038.

[3] Y.A. Antipov and V.V. Silvestrov, *Circular map for supercavitating flow in a multiply connected domain*, Quart. J. Mech. Appl. Math., 62 (2009), pp. 167–200.

[4] S. Bal, S.A. Kinnas, and H. Lee, *Numerical analysis of 2-d and 3-d cavitating hydrofoils under a free surface*, J. Ship Res., 45 (2001), pp. 34–49.

[5] P. Bassanini and A. Elcrat, *A univalent spiral-vortex model for separated flow past a polygonal obstacle*, ZAMP, 39 (1988), pp. 455–467.

[6] G. Birkhoff and E.H. Zarantonello, *Jets, Wakes, and Cavities*, Academic Press, New York, 1957.

[7] C.E. Brennen, *Cavitation and Bubble Dynamics*, Oxford University Press, Oxford, UK, 1985.

[8] G.P. Cherepanov, *Flow of an ideal fluid with free surface in doubly connected and triply connected regions*, J. Appl. Math. Mech., 27 (1964), pp. 1117–1124.

[9] D.A. Efros, *Hydrodynamical theory of two-dimensional flow with cavitation*, Comptes Rendus (Dokl. Akad. Nauk SSSR), 51 (1946), pp. 267–270.

[10] J.P. Franc and J.M. Michel *Fundamentals of Cavitation*, Kluwer Academic Publishers, New York, 2004.

[11] O. Furuya, *Nonlinear calculation of arbitrary shaped supercavitating hydrofoils near a free surface*, J. Fluid Mech., 68 (1975), pp. 21–40.

[12] D. Gilbarg and H.H. Rock, *On two theories of plane potential flows with finite cavities*, Memo. 8718, Naval Ordnance Lab., 1946.

[13] D. Gilbarg, *Jets and cavities*, Handbuch der Physic, 9, Springer-Verlag, Berlin, 1960, pp. 311–445.

[14] I.S. Gradshteyn and I.M. Ryzhik, *Tables of Integrals, Series, and Products*, Academic Press, San Diego, CA, 2000.

[15] T. Green and R.L. Street, *Two supercavitating hydrofoils near a free surface*, J. Fluid Mech., 27 (1967), pp. 1–28.

[16] M.I. Gurevich, *The Theory of Jets in an Ideal Fluid*, Nauka, Moscow, 1979.

[17] S.A. Kinnas and N.E. Fine, *A numerical nonlinear analysis of the flow around two- and three-dimensional partially cavitating hydrofoils*, J. Fluid Mech., 254 (1993), pp. 151–181.

[18] G. Kreisel, *Cavitation with finite cavitation numbers*, Admiralty Res. Lab. Rep. R1/H/36, 1946.

[19] B. Larock and R. Street, *Nonlinear solution for a fully cavitating hydrofoil beneath a free surface*, J. Ship Res., 11 (1967), pp. 131–140.

[20] H. Lemonnier and A. Rowe, *Another approach in modeling cavitating flow*, J. Fluid Mech., 195 (1988), pp. 557–580.
[21] A.R. Low, *Normal Elliptic Functions*, University of Toronto Press, Toronto, 1950.
[22] L.I. Sedov, *Two-Dimensional Problems in Hydrodynamics and Aerodynamics*, John Wiley & Sons, Inc., New York, 1965.
[23] A.G. Terent'ev, *Non-linear theory of cavitational flow around obstacles*, Fluid Dynam., 11 (1976), pp. 142–145.
[24] A.G. Terent'ev, *Mathematical Problems of Cavitation*, Chuvash. Gos. Univ., Cheboksary, 1981.
[25] L.N. Trefethen, *Numerical computation of the Schwarz–Christoffel transformation*, SIAM J. Sci. Stat. Comput., 1 (1980), pp. 82–102.
[26] M.P. Tulin, *Supercavitating flows—small perturbation theory*, J. Ship Res., 7 (1964), pp. 16–37.
[27] T.Y. Wu, *Cavity and wake flows*, Annu. Rev. Fluid Mech., 4 (1972), pp. 243–284.